OPEN

Citation: Cell Death and Disease (2014) 5, e1303; doi:10.1038/cddis.2014.266

www.nature.com/cddis

Retinal pigment epithelial cells undergoing mitotic catastrophe are vulnerable to autophagy inhibition

SY Lee[1,2,8], JS Oh[1,3,8], JH Rho[1,8], NY Jeong[1], YH Kwon[4], WJ Jeong[4], WY Ryu[4], HB Ahn[4], WC Park[4], SH Rho[4], YG Yoon[5], S-Y Jeong[6], YH Choi[7], HY Kim[1] and YH Yoo*[,1]

The increased mitochondrial DNA damage leads to altered functional capacities of retinal pigment epithelial (RPE) cells. A previous study showed the increased autophagy in RPE cells caused by low concentrations of rotenone, a selective inhibitor of mitochondrial complex I. However, the mechanism by which autophagy regulates RPE cell death is still unclear. In the present study, we examined the mechanism underlying the regulation of RPE cell death through the inhibition of mitochondrial complex I. We report herein that rotenone induced mitotic catastrophe (MC) in RPE cells. We further observed an increased level of autophagy in the RPE cells undergoing MC (RPE-MC cells). Importantly, autophagy inhibition induced nonapoptotic cell death in RPE-MC cells. These findings indicate that autophagy has a pivotal role in the survival of RPE-MC cells. We next observed PINK1 accumulation in the mitochondrial membrane and parkin translocation into the mitochondria from the cytosol in the rotenone-treated RPE-MC cells, which indicates that increased mitophagy accompanies MC in ARPE-19 cells. Noticeably, the mitophagy also contributed to the cytoprotection of RPE-MC cells. Although there might be a significant gap in the roles of autophagy and mitophagy in the RPE cells *in vivo*, our *in vitro* study suggests that autophagy and mitophagy presumably prevent the RPE-MC cells from plunging into cell death, resulting in the prevention of RPE cell loss.
Cell Death and Disease (2014) **5,** e1303; doi:10.1038/cddis.2014.266; published online 26 June 2014

Cell death is a process that is both complementary and antagonistic to cell division in order to maintain tissue homeostasis, and cell death has a pivotal role in several physiological processes and diseases.[1] The most extensively studied category, apoptosis, is characterized by the massive activation of caspases, chromatin condensation, and a reduction in cell volume. Necrosis is characterized by an increase in cell volume, the swelling of organelles, and the rupture of the plasma membrane and is largely considered an accidental, uncontrolled type of cell death.[2] Necroptosis is a regulated necrotic cell death that is triggered by broad caspase inhibition in the presence of death receptor ligands and is characterized by necrotic cell death morphology. Autophagy is a degradative lysosomal pathway that is characterized by the accumulation of cytoplasmic material in the vacuoles for bulk degradation by lysosomal enzymes. Although autophagy has a pivotal role in cell survival, increased autophagic activity is often associated with cell death.[2] Mitotic catastrophe (MC) is a type of cell death that results from a failure to undergo mitosis after DNA damage, leading to tetraploidy or endopolyploidy. Cells undergoing MC usually form large cells with multiple micronuclei.[3]

Retinal pigment epithelial (RPE) cells form a single layer of cells adjacent to the photoreceptor outer segment (POS) of the retina, and these cells have pivotal roles in the maintenance of the POS cells. RPE cell death is a significant factor in several ocular pathological conditions, such as age-related macular degeneration (AMD) and proliferative vitreoretinopathy (PVR). AMD is a progressive degeneration of the macula and is broadly classified as either dry or wet. The dry form of AMD is more common and is characterized by the presence of drusen in the macula. Mitochondrial DNA variants of respiratory complex I are associated with an increased risk of AMD.[4] Because damage to and the death of RPEs are crucial and perhaps even triggering events in AMD,[5] protection against RPE cell death could delay the onset of AMD. Conversely, RPE cells significantly contribute to the formation of the epiretinal membrane in PVR. Thus, the induction of RPE cell death in the epiretinal membranes could be a new approach to inhibit cellular proliferation in PVR.[6] Most studies concerning RPE cell death in the context of these ocular pathological conditions have focused on two types of cell death, apoptosis and necrosis.

Although advances have been made in the understanding of RPE cell death, there is little information concerning the role

[1]Department of Anatomy and Cell Biology, Dong-A University College of Medicine and Mitochondria Hub Regulation Center, Busan, South Korea; [2]Department of Rheumatology, Dong-A University College of Medicine, Busan, South Korea; [3]Bong Seng Memorial Hospital, Busan, South Korea; [4]Department of Ophthalmology, Dong-A University College of Medicine, Busan, South Korea; [5]Department of Biomedical Science, Jungwon University, Goesan, South Korea; [6]Department of Medical Genetics, Ajou University School of Medicine, Suwon, Republic of Korea and [7]Department of Biochemistry and Research Institute of Oriental Medicine, Dongeui University College of Oriental Medicine, Busan, South Korea

*Corresponding author: YH Yoo, Department of Anatomy and Cell Biology, Dong-A University College of Medicine and Mitochondria Hub Regulation Center, 3-1 Dongdaesin-Dong, Seo-Gu, Busan 602-714, South Korea Tel: +82 51 240 2926; Fax: +82 51 241 3767; E-mail: yhyoo@dau.ac.kr

[8]These authors contributed equally to this work.

Abbreviations: 3 MA, 3-methyladenine; AMD, age-related macular degeneration; Baf-A1, bafilomycin A1; CQ, chloroquine; JC-1, 5,5′,6,6′-tetrachloro-1,1′,3,3′-tetraethylbenzimidazol carbocyanine iodide; PVR, proliferative vitreoretinopathy; RPE, retinal pigment epithelial; RPE-MC, ARPE-19 cells undergoing mitotic catastrophe; zVAD-fmk, benzyloxylcarbonyl-Val-Ala-Asp-fluoromethylketone

Received 07.1.14; revised 20.3.14; accepted 20.5.14; Edited by M Piacentini

of autophagy in the RPE cell death associated with these ocular pathological conditions. Each day, RPE cells phagocytose and digest the distal parts of the POS, which are ultimately degraded in the lysosomes.[7–9] The interplay of phagocytosis and autophagy within the RPE is required for both POS degradation and the maintenance of retinoid levels to support vision.[9] In the RPE cells of old eyes, this physiological lysosomal load may be further increased to remove damaged material, and insufficient digestion of the damaged macromolecules and organelles by old RPE cells will lead to progressive accumulation of biological 'garbage', such as lipofuscin.[10] Thus, abnormalities in the lysosome-dependent degradation of shed POS debris can contribute to the degeneration of RPE cells. A previous study suggested that age-related changes in autophagy may underlie the genetic susceptibility found in AMD patients and may be associated with the pathogenesis of AMD.[10] However, the mechanism by which autophagy regulates RPE cell demise in AMD is still unclear. The role of autophagy in the proliferation of the RPE cells in PVR and its regulation as a therapeutic strategy for PVR have not been documented yet.

Rotenone, a natural isoflavonoid produced by plants, is a selective and stoichiometric inhibitor of mitochondrial complex I.[11] More specifically, rotenone blocks NADH oxidation by the NADH-ubiquinone oxide reductase enzymatic complex, which results in the inhibition of mitochondrial respiration and a reduction in ATP synthesis.[12–14] Rotenone treatment also results in the production of reactive oxygen species (ROS), eventually leading to cell death.[15,16] Several studies have shown that rotenone causes an accumulation of autophagic vacuoles, perhaps in response to the inhibition of mitochondrial function and the generation of oxidative stress.[17–19] Irrespective of that activity of rotenone has been lively studied in various cells, the effect of rotenone on RPE cells has rarely been studied. A previous study using an *in vitro* system revealed that low concentrations of rotenone resulted in mtDNA damage in RPE cells and suggested that the increased autophagy caused by rotenone treatment in aged RPE cells could affect the formation of drusen and AMD.[10] However, the mechanism by which rotenone regulates RPE cell demise remains unclear.

We undertook this study to elucidate the mechanism regulating the demise of RPE cells that are damaged by mitochondrial complex I inhibition. We report herein that rotenone induces MC in RPE cells. Additionally, we show that RPE cells undergoing mitotic catastrophe (RPE-MC cells) induced by mitochondrial complex I inhibition are vulnerable to autophagy inhibition.

Results

Rotenone induces MC in ARPE-19 RPE cells. Whereas rotenone treatment for 24 h did not reduce the viability of ARPE-19 cells, treatment for 72 h markedly reduced cell viability in a dose-dependent manner. Treatment with 2.5–25 μM rotenone for 48 h slightly (approximately 10–20%) decreased the viability of ARPE-19 cells (Figure 1a). Importantly, most of the ARPE-19 cells treated with 2.5–25 μM rotenone had multiple nuclei and an irregular shape (Figure 1b). Because 2.5 μM was the lowest dose that caused a slight decline in the viability of the ARPE-19 cells treated for 48 h, this concentration was used to further study the mechanism of the rotenone-induced cytotoxicity and the correlation between cell demise and rotenone-induced multinucleation. Flow cytometry analysis indicated that most rotenone-treated ARPE-19 cells became tetraploid (4C) by 48 h (Figure 1c). Because most cells contained $>$4N levels of DNA and were multinucleated, it seemed possible that these cells might be susceptible to death through MC. Therefore, we observed the cells under a transmission electron microscope. Transmission electron microscopy demonstrated the presence of micronuclei in the rotenone-treated cells (Figure 1d). These data indicate that rotenone induces MC in ARPE-19 cells.

Increased autophagy accompanies MC in ARPE-19 cells. We next examined whether rotenone increases autophagy in RPE-MC cells. Western blotting analysis demonstrated an increase in LC3-II levels in the rotenone-treated ARPE-19 cells (Figure 2a). Rotenone treatment did not alter the expression level of Beclin-1 or ATG5; however, rotenone slightly increased the expression level of VPS-34 in the ARPE-19 cells (Figure 2a). Rotenone decreased the interaction between Beclin-1 and Bcl-2 but increased the interaction between Beclin-1 and Vps-34 (Figure 2b). Flow cytometry analysis was used to observe and quantify the cells that contained organelles labeled with LysoTracker or acridine orange, and this analysis demonstrated that rotenone increased the development of acidic vesicular organelles (Figure 2c). Transmission electron microscopy showed that rotenone increased the number of autophagosomes in the RPE-MC cells (Figure 2d). These data indicate that increased autophagy is present in the RPE-MC cells.

RPE-MC cells are vulnerable to autophagy inhibition. We next examined whether inhibition of autophagy affects the viability of RPE-MC cells. Noticeably, autophagy inhibitors, such as 3-methyladenine (3 MA), bafilomycin A1 (Baf-A1), and chloroquine (CQ), significantly decreased their viability (Figure 3a). Next, the ARPE-19 cells were transfected with a green fluorescent protein (GFP)-LC3 fusion plasmid, treated with rotenone in the presence or absence of Baf-A1 or CQ, and then observed using confocal microscopy. After Baf-A1 or CQ treatment, the number of LC3-GFP puncta significantly increased (Figure 3b). Western blotting analysis showed that 3 MA prevented the accumulation of LC3-II in the rotenone-treated ARPE-19 cells. An autophagy flux assay, which was based on the evaluation of LC3-II turnover by western blotting analysis, showed that the prevention of lysosomal degradation by Baf-A1 or CQ induced the accumulation of LC3-II. Rotenone-alone treatment induced caspase-3 and -7 cleavage products. Rotenone, in conjunction with autophagy inhibition, also induced caspase-3 and -7 cleavage products. However, autophagy inhibition did not augment the accumulation of these cleavage products compared with the rotenone-alone treatment (Figure 3c), indicating that autophagy inhibition did not augment apoptosis. These data indicate that the inhibition of autophagy flux induces death of RPE-MC cells. We further examined whether autophagy inhibitors affect the

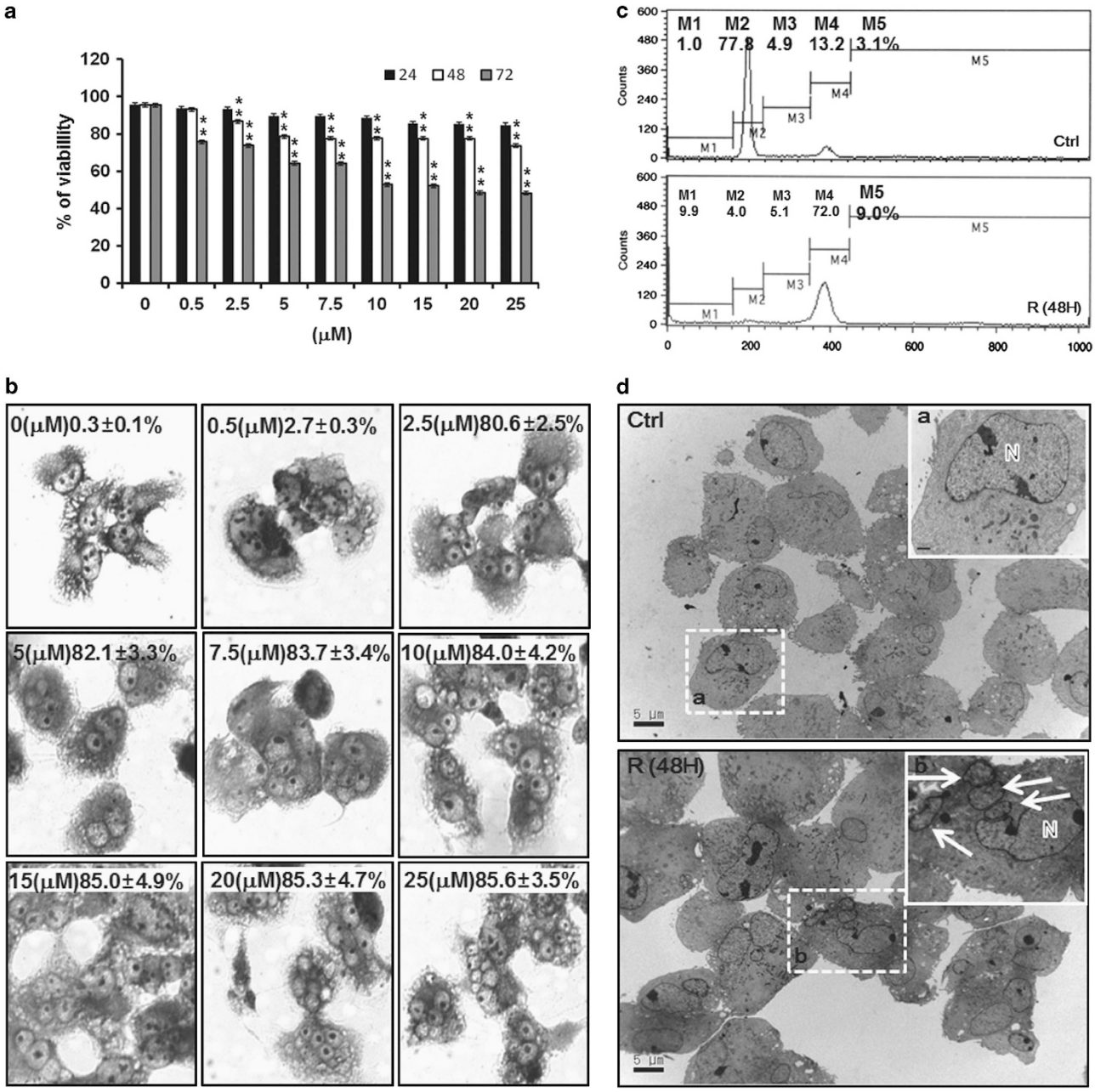

Figure 1 Rotenone induces mitotic catastrophe in ARPE-19 RPE cells. R, rotenone. (**a**) Viability assay, as determined by trypan blue exclusion. The values are expressed as the mean ± S.D. $^{**}P<0.01$ to the control. (**b**) Giemsa staining showing that ARPE-19 cells treated with rotenone have multiple nuclei. The numbers indicate the percentage of cells with multiple nuclei. The values are expressed as the mean ± S.D. (**c**) Flow cytometry analysis indicating that most rotenone-treated ARPE-19 cells were tetraploid by 48 h, as shown by a 4C DNA peak. Representative data are presented. (**d**) Transmission electron microscopy demonstrates the presence of micronuclei (arrows) in the rotenone-treated, multinucleated RPE cells. N, nucleus

rotenone-induced multinucleation. Our data indicate that autophagy inhibitors did not reverse the rotenone-induced multinucleation in the ARPE-19 cells (Figure 3d).

Augmentation of RPE-MC cell death by autophagy inhibition occurs through a nonapoptotic cell death pathway. We undertook several assays to determine the mechanism of cell death. Western blotting analysis demonstrated that caspase-3 and -7 were activated in the rotenone-alone-treated ARPE-19 cells (Figure 4a). Flow cytometry analysis demonstrated that the percentage of annexin V-positive cells was approximately 10% (Figure 4b). Additionally, incubation with benzyloxylcarbonyl-Val-Ala-Asp-fluoromethylketone (zVAD-fmk) completely prevented the cell death induced by the rotenone-alone treatment. However, zVAD-fmk only partially prevented the augmentation of cell death by the autophagy inhibitors (Figure 4c). A TUNEL (terminal deoxyribonucleotidyl transferase–mediated dUTP-digoxigenin nick end labeling) assay demonstrated that the autophagy inhibitors did not augment the percentage of

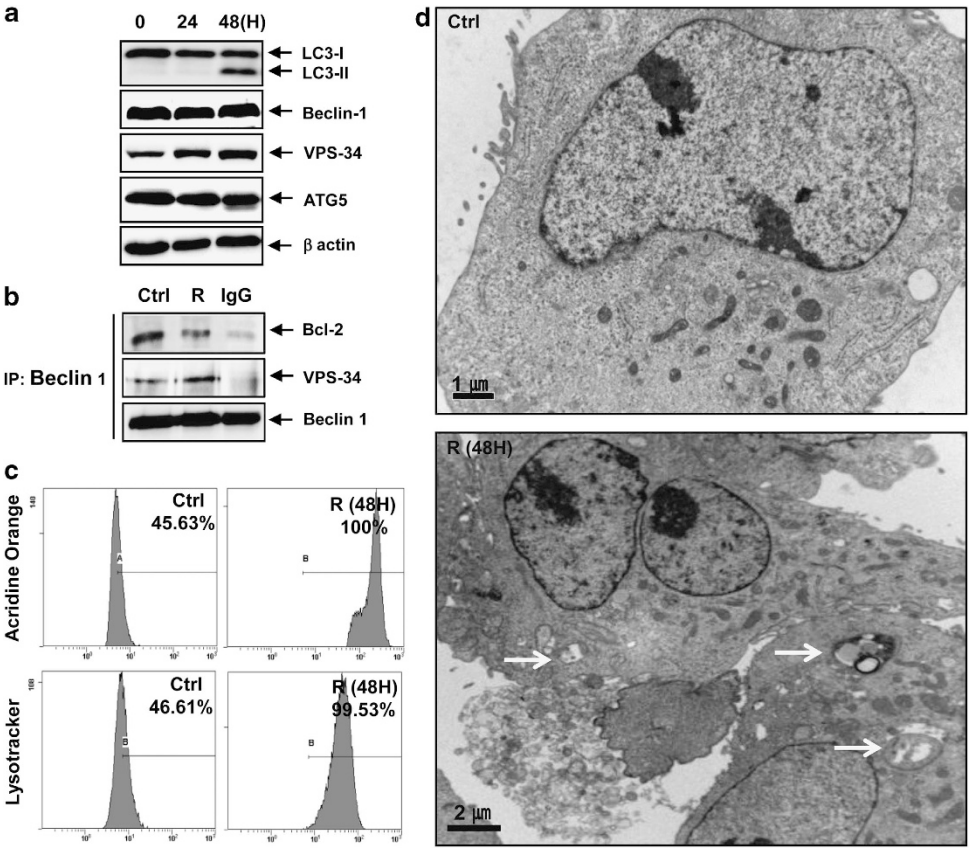

Figure 2 Increased autophagy occurs in the RPE-MC cells. C, control. (**a**) Western blotting analysis demonstrating an increase in the LC3-II levels in the rotenone-treated ARPE-19 cells. (**b**) Immunoprecipitated beclin-1 complex from the ARPE-19 cells. The interaction between beclin-1 and VPS-34 was increased, and the interaction between beclin-1 and Bcl-2 was decreased in the rotenone-treated cells compared with the control cells. (**c**) Flow cytometry analysis demonstrating that rotenone increased the development of acidic vesicular organelles. Representative data are presented. (**d**) Transmission electron microscopy showing that rotenone increased the number of autophagosomes or autophagolysosomes (arrows) in the RPE-MC cells

TUNEL-positive cells (Figure 4d). These data, in conjunction with Figure 3c, suggest that autophagy inhibition mainly induces nonapoptotic cell death in RPE cells undergoing rotenone-induced MC, whereas rotenone-alone treatment induces apoptotic cell death in RPE cells.

Parkin-mediated mitophagy occurs in the RPE-MC cells. We next examined whether mitophagy occurs in the RPE-MC cells. Western blotting analysis showed that rotenone markedly upregulated parkin protein. Parkin was absent in the mitochondria of the control cells but was translocated into the mitochondria of the rotenone-treated cells (Figure 5A). Rotenone also increased the amount of phosphorylated parkin (p-parkin) in the mitochondria. Although rotenone did not markedly upregulate PINK1, rotenone treatment increased the amount of PINK1 in the mitochondrial fraction. Flow cytometry analysis showed the reduction of MMP in the rotenone-treated cells (Figure 5B). Confocal microscopy differentiated the depolarized mitochondria, which showed moderate-to-low MitoTracker mitochondrial staining, from the normal mitochondria, which showed no dissipation of the mitochondrial membrane potential and thus displayed stronger staining. Parkin and PINK1 levels were significantly increased in the depolarized mitochondria (Figures 5C and D). Overexpression of both parkin and PINK1 increased the accumulation of LC3-II (Figure 5E). These findings indicate that parkin-mediated mitophagy occurs in the RPE-MC cells.

Mitophagy contributes to the cytoprotection of the RPE-MC cells. Because autophagy inhibitors reduced the viability of the RPE-MC cells, mitophagy appeared to underlie the autophagy-associated protection of the rotenone-treated RPE cells. To verify that mitophagy has a cytoprotective role, we examined the effect of parkin depletion on cell death. Parkin knockdown partially prevented the rotenone-induced increase in LC3-II level (Figure 6A). Noticeably, parkin knockdown significantly aggravated the RPE cell death induced by rotenone treatment alone (Figure 6B). These findings indicate that mitophagy has a role in the survival of the RPE-MC cells. Transmission electron microscopy revealed the presence of degraded mitochondria and autophagosomes in the rotenone-treated cells. Mitochondria merged with lysosomes were also observed in the RPE-MC cells (Figures 6Ca–Cd), indicating active mitophagy in the RPE-MC cells. There were no autophagosomes or lysosomes observed in the RPE-MC cells treated with rotenone and 3 MA, and in these cells, the degraded mitochondria were left undigested (Figure 6Cd). There were numerous autophagosomes in the RPE-MC cells

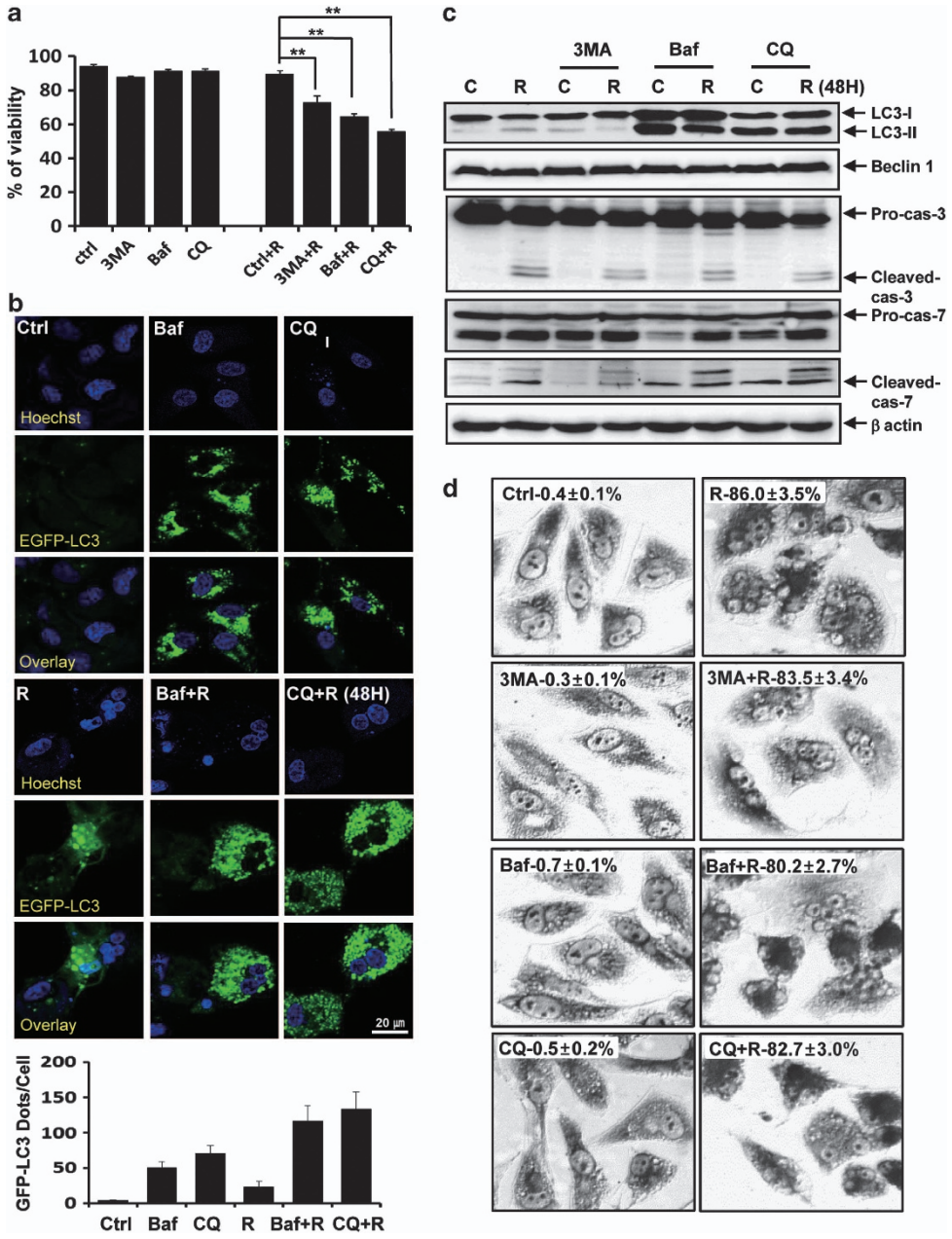

Figure 3 RPE-MC cells are vulnerable to autophagy inhibition. The values are expressed as the mean ± S.D. (**a**) Viability assay showing that autophagy inhibition augments the reduction of viability caused by rotenone treatment. $^{**}P<0.01$. (**b**) Autophagy flux assay indicating that autophagy inhibitors blocked autophagy flux. (**c**) Western blotting analysis demonstrating that autophagy inhibitors induced the accumulation of LC3-II without augmenting apoptosis. (**d**) Giemsa staining showing that autophagy inhibitors did not reverse the rotenone-induced multinucleation. The numbers indicate the percentage of cells with multiple nuclei. The values are expressed as the mean ± S.D. See Figure 2 for other definitions

treated with rotenone and Baf-A1 or CQ, and numerous degraded mitochondria were present and separate from the autophagosomes (Figures 6Ce and Cf). These findings indicate that autophagy inhibitors blocked the removal of the degraded mitochondria in the RPE-MC cells. These findings prove that parkin-mediated mitophagy underlies the autophagy-associated cytoprotection of the RPE-MC cells.

Alpha B crystallin (αB-crystallin) protects RPE-MC cells from apoptosis. Because αB-crystallin is the principal antiapoptotic factor in RPE cells,[20,21] we examined whether αB-crystallin exerts antiapoptotic effects in RPE-MC cells. αB-crystallin knockdown significantly augmented the reduction in RPE-MC cell viability compared with cells treated with rotenone alone (Figure 7a). These data indicate that αB-crystallin prevents RPE-MC cells from plunging into cell death. Noticeably, TUNEL assay showed that αB-crystallin knockdown induced apoptosis in RPE cells treated with autophagy inhibitors (Figure 7b), indicating that αB-crystallin exerts antiapoptotic activity in the RPE cells

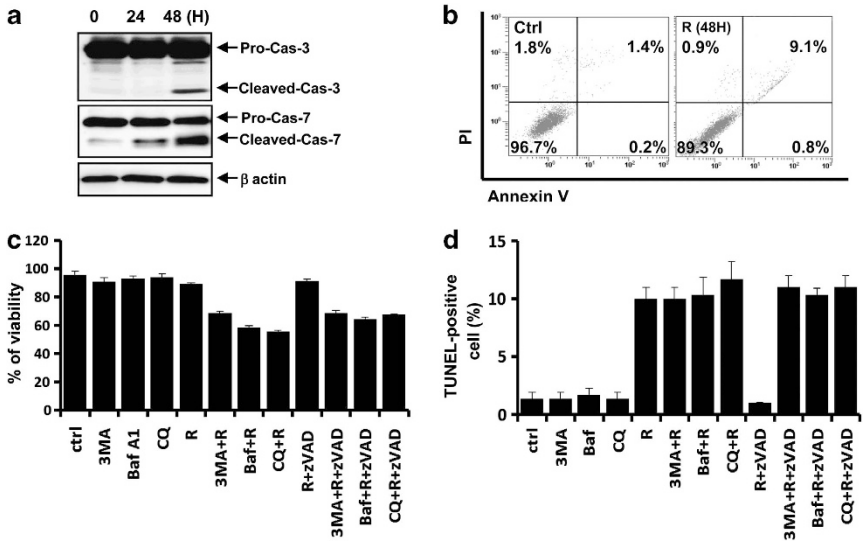

Figure 4 Augmentation of RPE-MC cell death by autophagy inhibition occurs through a nonapoptotic cell death pathway. (**a**) Western blotting analysis demonstrating that caspase-3 and -7 were activated in the rotenone-alone-treated ARPE-19 cells. (**b**) Flow cytometry analysis demonstrating that the percentage of annexin V-positive cells was approximately 10%. Representative data are presented. (**c**) Viability assay showing that zVAD-fmk only partially prevented the augmentation of cell death caused by the autophagy inhibitors. The values are expressed as the mean ± S.D. (**d**) TUNEL assays showing that autophagy inhibitors did not augment the percentage of TUNEL-positive cells. See Figure 2 for other definitions. The values are expressed as the mean ± S.D.

prone to cell death due to autophagy inhibition. Flow cytometry analysis showed that αB-crystallin knockdown resulted in a markedly increased accumulation of annexin V-positive RPE-MC cells, indicating that αB-crystallin knockdown caused the autophagy inhibition-induced death of RPE-MC cells to change direction from a nonapoptotic cell death to an apoptotic cell death (Figure 7c). These findings suggest that αB-crystallin exerts antiapoptotic activity in RPE-MC cells, preventing them from experiencing apoptosis.

Discussion

The present study showed that low concentrations of rotenone induced MC in RPE cells. Although only one previous study reported that rotenone-induced MC is associated with cancer cell death,[22] the mechanism underlying rotenone-induced MC has not been fully documented yet. The toxicity of rotenone mainly results from the inhibition of complex I in the mitochondrial respiratory chain. However, it is not clear whether the induction of MC by rotenone also depends on the same activity of rotenone. Only one previous study supports the possibility that rotenone induces polyploidization by inhibiting mitochondrial respiratory complex I; this study demonstrated the high likelihood of polyploidization in head and neck paragangliomas with inactivating mutations in mitochondrial respiratory complex.[23] We further observed that DPI, another mitochondrial respiration complex I inhibitor, induced MC and that silencing against mitochondrial complex I induced MC in ARPE-19 cells (Supplementary Figures S1a and S2). In contrast, a mitochondrial complex III inhibitor antimycin A did not induce MC in ARPE-19 cells (Supplementary Figure S3). Thus we presume that the observed phenotypes in rotenone-treated ARPE-19 cells are specifically mediated by mitochondrial respiration complex I inhibition. The other major mechanism of rotenone toxicity involves the production of ROS, which eventually leads to cell death.[15,16] However, it was reported that the MC-inducing effect of rotenone in cancer cells was not dependent on the production of ROS.[22] To obtain a more objective and detailed view of rotenone-induced MC, further studies should be undertaken to distinguish MC as a specific response in certain cell types and in response to certain drugs.

Arguably, the most intriguing finding of this study is that RPE-MC cells are vulnerable to autophagy inhibition. The augmentation of ARPE-19 cell death by autophagy inhibition were also observed in DPI-treated ARPE-19 cells (Supplementary Figures S1b–e). To date, few previous studies have examined the role of autophagy in cells undergoing MC. Depending on those previous studies, increased autophagy may accompany MC, the induction of autophagy may potentiate the cell death undergoing MC, or autophagy inhibition may prevent the formation of polyploid cells.[24,25] Importantly, we first demonstrated that autophagy inhibition induced cell death in polyploid cells. Previous studies showed that MC cells are prone to cell death. However, it has been proposed that MC might not even constitute a *bona fide* cell death executioner mechanism but an oncosuppressive pathway that precedes and is distinct from, yet operates through, cell death or senescence.[26,27] MC makes tumor cells more unstable and vulnerable to chemotherapy, supporting that induction of MC may provide a new approach to cancer therapy.[28] Conversely, polyploid cells may be resistant to DNA-damaging agents.[27,29,30] Thus the inhibition of MC by blocking autophagy could be a strategy to enhance the therapeutic efficacy.[24,28] Although there might be a significant gap in the role which autophagy plays in RPE cells *in vivo*, our *in vitro* study suggests that autophagy presumably prevent RPE-MC cells from plunging into cell death, resulting in the prevention of RPE cell loss *in vivo*. Our findings illuminate the possibility of clinical application by providing a working model

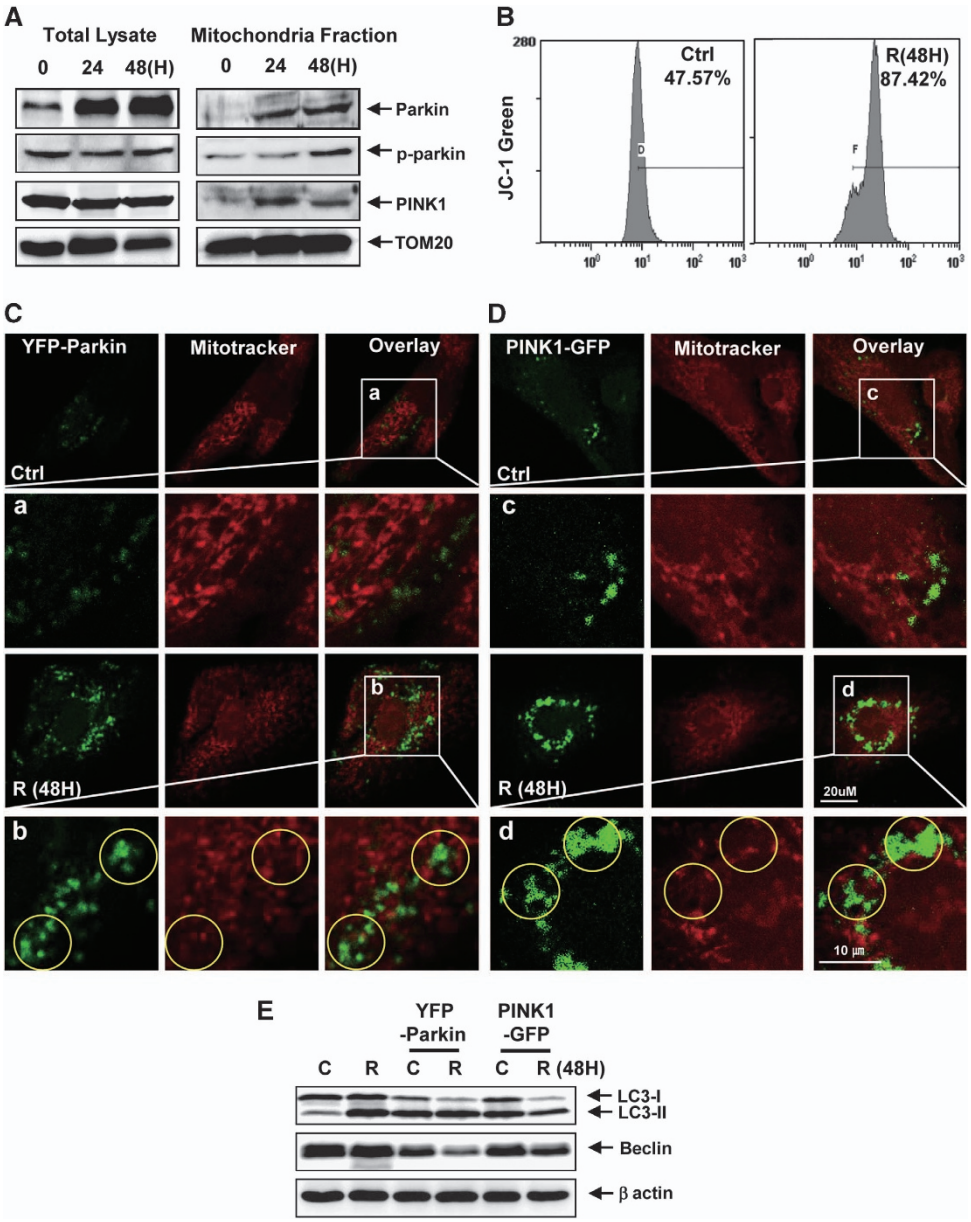

Figure 5 Parkin-mediated mitophagy occurs in the RPE-MC cells. (**A**) Western blotting analysis demonstrating the mitochondrial translocation of parkin and mitochondrial accumulation PINK1 in the rotenone-treated RPE cells. (**B**) Flow cytometry analysis demonstrating the reduction of MMP in the rotenone-treated cells. Representative data are presented. (**C**) Confocal microscopy showing that overexpressed parkin-YFP selectively translocated to the depolarized mitochondria (yellow circles). (**D**) Confocal microscopy showing that overexpressed PINK1-GFP selectively located to the depolarized mitochondria (yellow circles). (**E**) Western blotting analysis demonstrating that the overexpression of both parkin and PINK1 led to an increase in LC3-II. See Figure 2 for other definitions

for the prevention of RPE cell death by increasing autophagy or the augmentation of RPE cell death by inhibiting autophagy.

Mitochondria can cause normal cell dysfunction owing to a number of problems that can occur at any time, such as oxidative stress or mutations in the mitochondrial genome,[31] which can occur in the metabolic pathway that is mediated by the mitochondrial respiratory chain complexes. Thus the mitochondria need to remain functional through several mechanisms, because their function is tightly linked to the homeostasis of the cells. Mitophagy is one of the mechanisms that regulate mitochondrial quality control.[32–34] Mitophagy, a mechanism to eliminate dysfunctional mitochondria through autophagy, is essential for a variety of cellular events. Mitophagy is involved in the selective clearance of damaged and dysfunctional mitochondria from the intact normal mitochondrial network and in the recycling of the degraded compounds. The selective engulfment of impaired mitochondria during mitophagy is initially mediated by two proteins, PINK1 and parkin.[35,36] These two proteins have fundamental roles in the selective autophagic elimination of damaged mitochondria from the cells. The present study demonstrated that rotenone-induced mitophagy is also mediated via PINK1-mediated

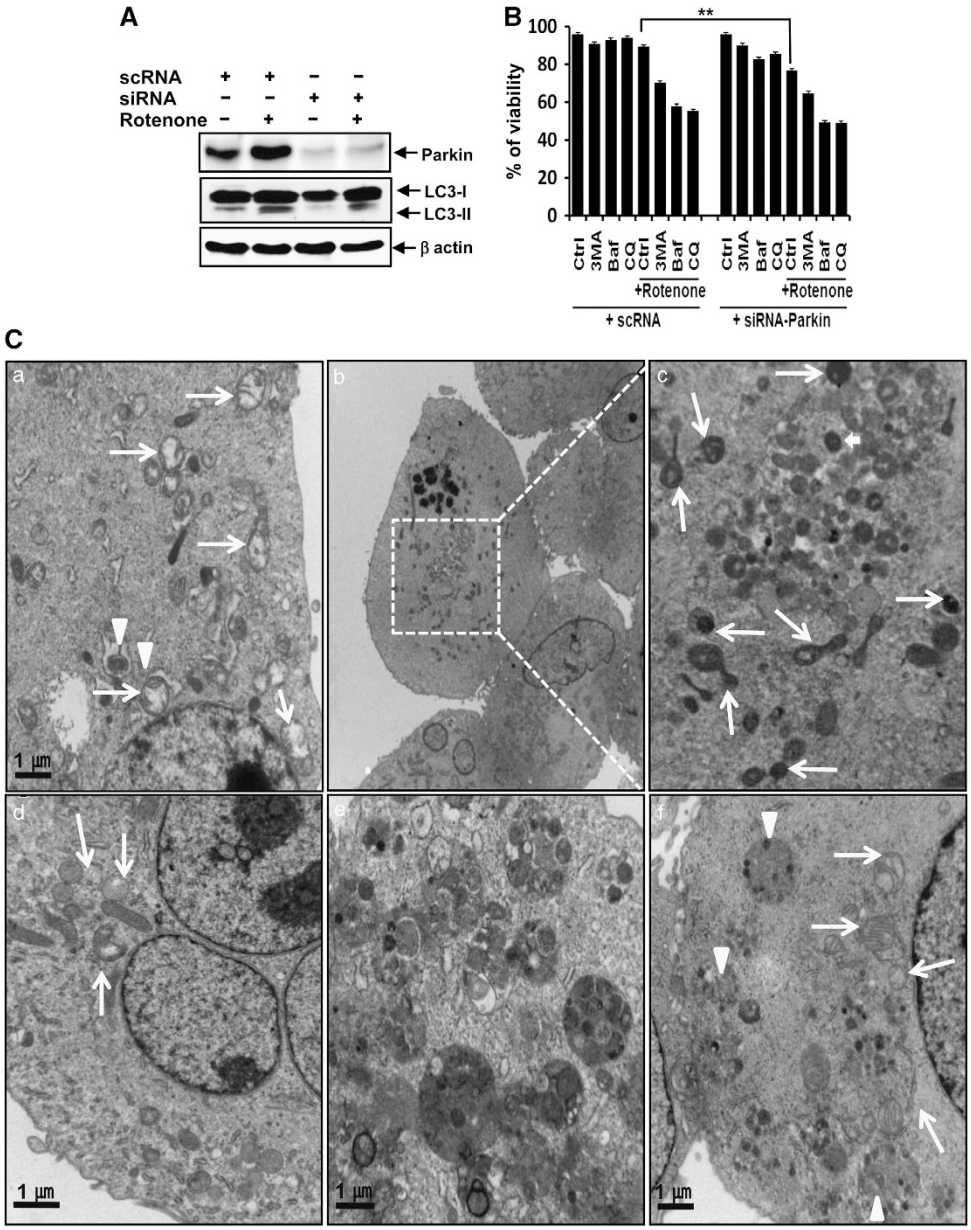

Figure 6 Mitophagy contributes to the cytoprotection of RPE-MC cells. (**A**) Western blotting analysis demonstrating that parkin knockdown partially prevented the rotenone-induced increase in LC3-II. (**B**) Viability assay showing that parkin knockdown significantly aggravated the RPE cell death induced by rotenone treatment. The values are expressed as the mean ± S.D. $^{**}P < 0.01$. (**C**) Transmission electron microscopy, (a–c). Rotenone-alone-treated cells. Degraded mitochondria (arrows), autophagosomes (arrow head), and mitochondria merged with lysosomes (white arrows) are observed. (d) RPE-MC cells treated with rotenone and 3-MA. The degraded mitochondria (arrows) are left undigested. (e) RPE-MC cells treated with rotenone and CQ. Numerous autophagosomes (arrow heads) are scattered throughout the cytosol. Similar findings were observed in the Baf-A1–treated cells (data not shown). (f) RPE-MC cells treated with rotenone and Baf-1. Numerous degraded mitochondria (arrows) are shown separate from the autophagosomes (arrow heads). Similar findings were observed in the CQ-treated cells (data not shown). See Figure 2 for other definitions

parkin translocation into the nonfunctional mitochondria of the RPE-MC cells. Furthermore, our data suggest that PINK1/parkin-mediated mitophagy underlies the cytoprotection of the RPE-MC cells.

Although we elucidated the mechanism underlying the rotenone-treated RPE cell death, it is not yet clear that this mechanism accurately describes the *in vivo* events pertaining to the therapeutics for PVR patients or the pathogenesis of AMD. To date, no report has demonstrated that pharmacological approach toward inhibiting cellular proliferation in PVR induces RPE-MC cells. Thus, possible antiproliferative efficacy of rotenone in conjunction with autophagy inhibitors for PVR patients needs to be verified by further future studies. Further, separating supposedly desirable effects of rotenone from retinotoxic side-effects should be investigated further. It is not clear that mitochondrial complex 1 inhibition-induced cell death is relevant to RPE cell loss in AMD patients, although the data obtained

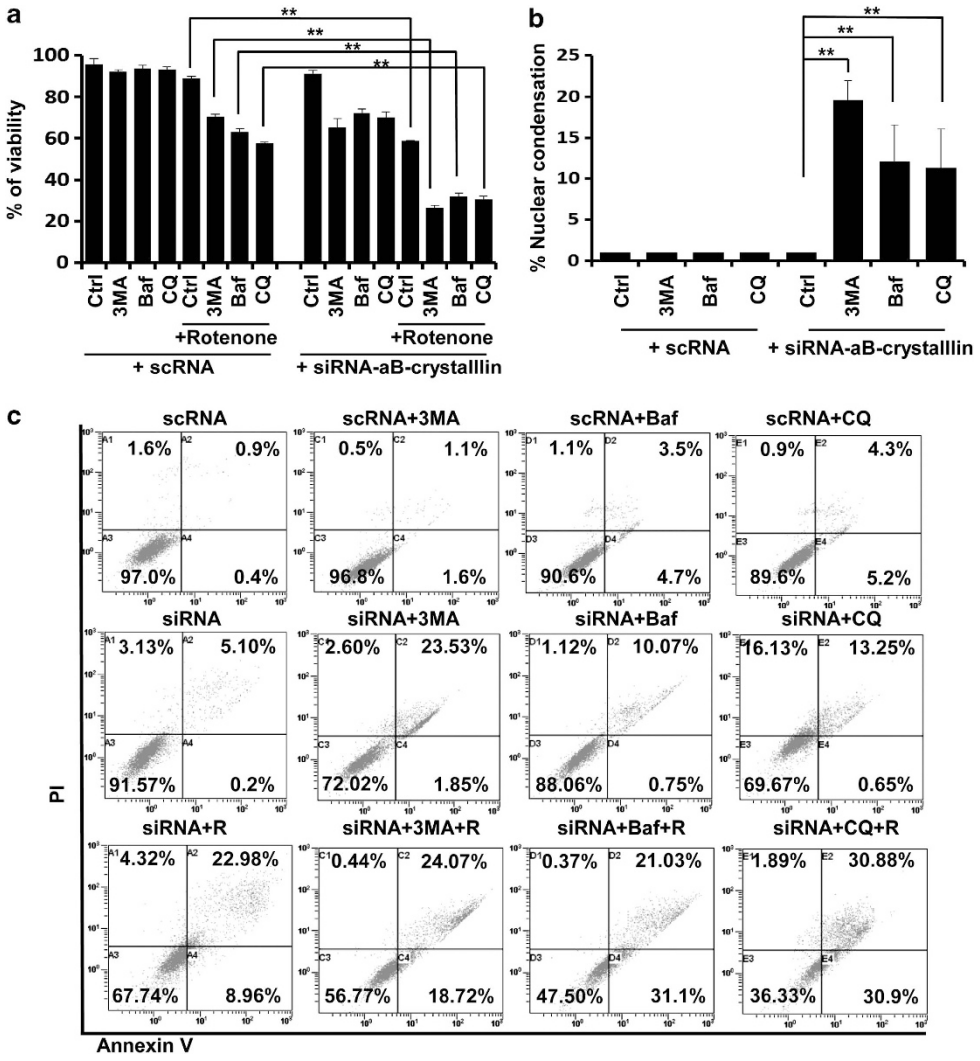

Figure 7 Alpha B crystallin protects RPE-MC cells from apoptosis. (**a**) Viability assay showing that αB-crystallin knockdown augmented the rotenone-induced ARPE-19 cell death. The transfection mixture was added to each well and incubated for 4 h. Then 2 ml of growth medium was added, and the cells were incubated for an additional 20 h. After the siRNA transfection medium was removed, each well was washed in phosphate-buffered saline solution. The cells were treated with various concentrations of rotenone for 48 h. $^{**}P<0.01$. The values are expressed as the mean ± S.D. (**b**) TUNEL assay showing that αB-crystallin knockdown induced apoptosis in the RPE cells treated with autophagy inhibitors. The values are expressed as the mean ± S.D. $^{**}P<0.01$. (**c**) Flow cytometry analysis demonstrating that αB-crystallin knockdown resulted in a markedly increased accumulation of annexin V-positive cells. Representative data are presented. See Figure 2 for other definitions

from the *in vitro* experimental system are relevant to the formation of drusen and AMD.[10] As no study has demonstrated the presence of RPE-MC cells to date, it is not certain yet that MC involves in the pathogenesis of AMD. A previous histological analysis of retinas from AMD patients revealed the presence of multinucleated giant cells disrupting the RPE,[37] and another study showed that mutation of hemicentin-1 that is localized to the cytokinetic furrow[38] was linked to AMD. Moreover, polyploidization frequently accompanies aging,[39] and mitochondrial DNA damage increased in rodent RPEs/choroids with age.[40] Taken together with these reports, we can cautiously assume the possible involvement of mitochondrial respiration complex 1 inhibition-induced MC of RPE cells in the pathogenesis of AMD. This hypothesis also needs to be verified by further future studies.

In conclusion, rotenone induced MC in RPE cells and RPE-MC cells were vulnerable to autophagy inhibition.

Materials and Methods

Reagents. The following reagents were obtained commercially: rabbit polyclonal anti-human Bcl-2, Tom20, GFP, YFP, p-Parkin, and mouse monoclonal anti-human Parkin and Beclin-1 antibodies from Santa Cruz Biotechnology (Santa Cruz, CA, USA); rabbit polyclonal anti-human caspase-3, caspase-7, LC3B, HRP-conjugated donkey anti-rabbit, sheep anti-mouse IgG antibodies, and RIPA buffer from Cell Signaling (Danvers, MA, USA); rabbit polyclonal anti-human PINK1 from Abcam, Cambridge, UK; FITC-conjugated goat anti-rabbit and Texas Red-conjugated horse anti-mouse IgGs from Vector (Burlingame, CA, USA); Dulbecco's modified Eagle's medium (DMEM)/F12, Opti-MEM, and penicillin–streptomycin from Gibco BRL (Gaithersburg, MD, USA); LysoTracker and Lipofectamine from Invitrogen (Carlsbad, CA, USA); β-actin antibody, Hoechst 33342, dimethyl sulfoxide (DMSO), RNase A, proteinase K, propidium iodide (PI), protein-A agarose, 3-methyladenine (3MA), Baf-A1, annexin V-FITC apoptosis detection kit, Mdivi-1, acridine orange, CQ,

and rotenone from Sigma (St. Louis, MO, USA); pan caspase inhibitor from Calbiochem (San Diego, CA, USA); 5,5′,6,6′-tetrachloro-1,1′,3,3′-tetraethylbenzimidazol carbocyanine iodide (JC-1) from Molecular Probes (Eugene, OR, USA); SuperSignal WestPico enhanced chemiluminescence western blotting detection reagent and fetal bovine serum (FBS) from Thermo (Logan, UT, USA); and siPORT Amine from Ambion (Austin, TX, USA).

Cell culture. The ARPE-19 cells were purchased from the American Type Culture Collection (ATCC, Rockville, MD, USA) and were maintained at 37 °C with 5% CO_2 in an air atmosphere; the cells were grown in a 1 : 1 mixture of DMEM and Ham F12 medium supplemented with 10% FBS.

Rotenone treatment. Twenty-four hours after the ARPE-19 cells were subcultured, the original medium was removed. The cells were washed with PBS and then incubated in the same fresh medium. Rotenone was added from a stock solution into the media to obtain 2.5-μM dilutions of the drug. After 0, 24, 48, 72, or 96 h, the cells were harvested, stained with trypan blue, and then counted using a hemocytometer. The concentration of PBS used in this study had no effect on ARPE-19 cell proliferation in our preliminary studies.

Giemsa staining. ARPE-19 cells were cultured without or with rotenone and were then fixed with methanol for 10 min. For nuclear morphology observation, slides were stained for 15 min with Giemsa solution.

Quantification of DNA hypoploidy and cell cycle phase analysis by flow cytometry. Ice-cold 95% ethanol supplemented with 0.5% Tween-20 was added to cell suspensions to a final concentration of 70% ethanol. The fixed cells were pelleted and washed in 1% BSA–PBS solution. The cells were resuspended in 1 ml of PBS containing 11 Kunitz U/ml RNase and were incubated at 4 °C for 30 min, washed once with BSA–PBS, and resuspended in a 50 μg/ml PI solution. The cells were incubated at 4 °C for 30 min in the dark and were then filtered through 35 mm mesh, and the DNA content was determined using a FACSCalibur (Becton-Dickinson, San Jose, CA, USA) flow cytometer within 1 h of staining. The cellular DNA content was analyzed using the CellQuest software (Becton-Dickinson).

Co-immunoprecipitation. Cell extracts were incubated with the appropriate antibodies in extraction buffer at 4 °C overnight. Immunocomplexes were precipitated using protein A-sepharose beads for 2 h and were washed five times with extraction buffer before boiling in sodium dodecyl sulfate (SDS) sample buffer. The immunoprecipitated proteins or aliquots containing 40 μg protein were separated on SDS-polyacrylamide gels, and the western blotting analysis was performed as described. Each co-immunoprecipitation experiment was confirmed through reciprocal immunoprecipitation.

Human parkin and PINK1 siRNA. Human Parkin siRNA (SMART pool; L-003603-00-0005) and PINK1 siRNA (SMART pool; L-004030-00-0020) were purchased from Thermo Scientific (Hudson, NH, USA). As a negative control, the same nucleotides were scrambled to form nongenomic combinations.

siRNA transfection. siRNA transfection was performed using siPORT Amine and Opti-MEM media. The cells were grown to 40–50% confluent in six-well plates and were transfected with a final siRNA concentration of 100 nM per well. The transfection mixture was added to each well, and the cells were incubated for 4 h. Then 2 ml of growth medium was added, and the cells were incubated for another 20 h. After siRNA transfection, the medium was removed, and each well was washed in PBS solution.

Subcellular fractionation. ARPE-19 cells (10^7 cells/well) were washed in Tris-based Mg^{2+}/Ca^{2+}-deficient buffer (135 mM NaCl, 5 mM KCl, and 25 mM Tris, pH 7.6) and were allowed to swell for 10 min in ice-cold hypotonic CaRSB buffer (10 mM NaCl, 1.5 mM $CaCl_2$, 10 mM Tris, pH 7.5, and 1x protease inhibitor cocktail). The cells were disrupted by 60 strokes in a Dounce homogenizer (Thomas Scientific, Swedesboro, NJ, USA), and mitochondria stabilization buffer (210 mM mannitol, 70 mM sucrose, 5 mM EDTA, and 5 mM Tris, pH 7.6) was added to stabilize the mitochondria. After collecting the nuclei by centrifuging the cells twice at 3000 r.p.m. for 15 min, the supernatant was spun at 14 000 r.p.m. for 20 min at 4 °C. The pellet and the supernatant included the mitochondrial and cytoplasmic fractions, respectively. Cells (5×10^7) were swollen in ice-cold hypotonic CaRSB buffer and were disrupted using a Dounce homogenizer. Cell homogenates were then spun down twice at 3000 r.p.m. for 15 min.

Western blotting analysis. The cells were washed twice with ice-cold PBS, resuspended in 200 μl of ice-cold solubilizing buffer (300 mM NaCl, 50 mM Tris-HCl [pH 7.6], 0.5% Triton X-100, 2 mM PMSF, 2 μl/ml aprotinin, and 2 μl/ml leupeptin), and incubated at 4 °C for 30 min. The lysates were centrifuged at 14 000 r.p.m. for 15 min at 4 °C. The protein concentrations of the cell lysates were determined using the Bradford protein assay kit (Bio-Rad, Richmond, CA, USA), and equivalent amounts of protein were loaded onto 7.5–15% SDS-polyacrylamide gel electrophoresis gels. The proteins were then transferred onto a nitrocellulose membrane (Amersham Pharmacia Biotech, Piscataway, NJ, USA) and were probed using each antibody. Immunostaining with the antibodies was performed using an enhanced chemiluminescence substrate (SuperSignal WestPico; Pierce, Rockford, IL, USA) and was detected using photographic film (LAS-3000 Plus; Fuji Photo Film Co. Ltd, Tokyo, Japan). Equivalent protein loading was confirmed by Ponceau S staining.

Transfection of LC3-GFP, YFP-parkin, and PINK1-GFP into ARPE-19 cells and confocal microscopy. The mammalian expression construct of human LC3 cloned into pEGFP was provided by Dr. N Mizushima (Tokyo Medical and Dental University, Tokyo, Japan). YFP hparkin and GFP hPINK1 were provided by Dr. J Chung (Seoul National University, Seoul, Korea). The ARPE-19 cells were seeded in six-well plates (10^5 cells/well) and were transiently transfected with each construct using Lipofectamine 2000, according to the manufacturer's instructions. Briefly, 2 μg of plasmid DNA was mixed with 6 μl of Lipofectamine 2000 and then incubated with Opti-MEM. The plasmid DNA–Lipofectamine 2000 complex was added to the cells, and the mixture was further incubated for 4 h at 37 °C. After incubation, the medium was replaced with 2 ml of growth medium, and the cells were maintained for an additional 20 h. Twenty-four hours after transfection, the plasmid DNA transfection medium was removed, and each well was washed with PBS solution. The cells were treated as indicated and fixed with 4% paraformaldehyde for 15 min at 4 °C. Fluorescent images were obtained and analyzed using a Zeiss LSM 510 laser-scanning confocal microscope (Zeiss, Gőettingen, Germany). To quantify those cells that showed a punctuate pattern, at least 300 cells from each experiment were counted by an observer who was blinded to the experimental group.

Transmission electron microscopy. Forty-eight hours after treatment, the cells were harvested, pelleted, and fixed in 2.5% glutaraldehyde in phosphate buffer. After the cells were rinsed with phosphate buffer, the samples were postfixed in 1% osmium tetroxide for 1 h, rinsed with water, dehydrated in a graded ethanol series, incubated with propylene oxide, and kept overnight in Epon812. The samples were embedded in Epon812 and cured in an oven at 60 °C. Ultrathin sections were obtained using a EM UC7 microtome (Leica, Wien, Austria). The sections were stained with uranyl acetate and lead citrate and were observed using a H-7650 transmission electron microscope (Hitachi, Tokyo, Japan). For each treatment or control group, at least 200 cells from randomly chosen transmission electron microscopy fields were observed.

TUNEL staining. To observe the cells undergoing apoptosis, the fluorescent TUNEL assay was performed using an *in situ* death detection kit. Briefly, cells that had been grown on coverslips were fixed in 4% paraformaldehyde for 15 min and then rinsed in PBS. After the cells were incubated with terminal deoxynucleotidyl transferase (TdT) enzyme for 1 h at 37 °C, anti-digoxigenin-FITC was applied for 30 min at room temperature. The nuclei were counterstained with propidium iodide/antifade. Fluorescent images were observed and analyzed using a Zeiss LSM 510 laser-scanning confocal microscope. The total cell number, at least 300 cells from each experiment, was counted, and the number of cells showing positive staining was calculated under epifluorescence optics by a blinded observer.

Hoechst staining. Cells were harvested, and the cell suspension was centrifuged onto a clean, fat-free glass slide using a Cellspin (Hanil Science, Incheon, South Korea). The samples were stained with 4 μg/ml Hoechst 33342 for 30 min at 37 °C and were fixed for 10 min in 4% paraformaldehyde. The total cell number, at least 300 cells from each experiment, was counted under DIC optics, and the number of cells showing condensed or fragmented nuclei in Hoechst staining was calculated under epifluorescence optics by a blinded observer.

Flow cytometric measurement of apoptosis, organellar contents, and mitochondrial membrane potential. For quantitation of the acidic organellar contents, the cells were incubated in 50 nM LysoTracker Red or 1 μg/ml acridine orange for 30 min at 37 °C. For quantitation of the apoptotic cells, the cells were incubated with 500 μl of annexin V-binding buffer containing 5 μl of annexin V-FITC conjugate and 10 μl of propidium iodide solution. After incubating for 10 min at room temperature, the cells were analyzed by flow cytometry. For measurement of the mitochondrial membrane potential, the cells were incubated with 4 μg/ml JC-1 for 30 min at 37 °C. Data were acquired and analyzed with ADC XL (Beckman Coulter, Miami, FL, USA).

Statistical analysis. At least $\geq$3 independent experiments were carried out *in vitro*. The results are expressed as the mean ± S.D. from three experiments. The results of the experimental and control groups were tested for statistical significance using the Student's *t*-test. In all cases, a *P*-value <0.05 was considered significant.

Conflict of Interest

The authors declare no conflict of interest.

Acknowledgements. This work was supported by the National Research Foundation of Korea (NRF) grant funded by the Korea government (MSIP) (2013 041811).

Author contributions

YGY, SYJ, YHC, HYK and YHY designed the research. SYL, JSO and NYJ co-wrote the manuscript. JHR, YHK, WJJ, WYR, HBA, WCP and SHR contributed experimentally.

1. Dunai Z, Bauer PI, Mihalik R. Necroptosis: biochemical, physiological and pathological aspects. *Pathol Oncol Res* 2011; **17**: 791–800.
2. Kroemer G, Levine B. Autophagic cell death: the story of a misnomer. *Nat Rev Mol Cell Biol* 2008; **9**: 1004–1010.
3. Castedo M, Perfettini JL, Roumier T, Andreau K, Medema R, Kroemer G. Cell death by mitotic catastrophe: a molecular definition. *Oncogene* 2004; **23**: 2825–2837.
4. SanGiovanni JP, Arking DE, Iyengar SK, Elashoff M, Clemons TE, Reed GF *et al.* Mitochondrial DNA variants of respiratory complex I that uniquely characterize haplogroup T2 are associated with increased risk of age-related macular degeneration. *PLoS One* 2009; **4**: e5508.
5. Zarbin MA. Age-related macular degeneration: review of pathogenesis. *Eur J Ophthalmol* 1998; **8**: 199–206.
6. Kim J, Bae HR, Park BS, Lee JM, Ahn HB, Rho JH *et al.* Early mitochondrial hyperpolarization and intracellular alkalinization in lactacystin-induced apoptosis of retinal pigment epithelial cells. *J Pharmacol Exp Ther* 2003; **305**: 474–481.
7. Bok D. The retinal pigment epithelium: a versatile partner in vision. *J Cell Sci Suppl* 1993; **17**: 189–195.
8. Strauss O. The retinal pigment epithelium in visual function. *Physiol Rev* 2005; **85**: 845–881.
9. Kim JY, Zhao H, Martinez J, Doggett TA, Kolesnikov AV, Tang PH *et al.* Noncanonical autophagy promotes the visual cycle. *Cell* 2013; **154**: 365–376.
10. Wang AL, Lukas TJ, Yuan M, Du N, Tso MO, Neufeld AH. Autophagy and exosomes in the aged retinal pigment epithelium: possible relevance to drusen formation and age-related macular degeneration. *PLoS One* 2009; **4**: e4160.
11. Oberg KE. The inhibition of the respiration of brain mitochondria of rotenone-poisoned fish. *Exp Cell Res* 1964; **36**: 407–410.
12. Blandini F, Nappi G, Greenamyre JT. Quantitative study of mitochondrial complex I in platelets of Parkinsonian patients. *Mov Disord* 1998; **13**: 11–15.
13. Fang N, Casida JE. Cube resin insecticide: identification and biological activity of 29 rotenoid constituents. *J Agric Food Chem* 1999; **47**: 2130–2136.
14. Sestili P, Brambilla L, Cantoni O. Rotenone and pyruvate prevent the tert-butylhydroperoxide-induced necrosis of U937 cells and allow them to proliferate. *FEBS Lett* 1999; **457**: 139–143.
15. Li N, Ragheb K, Lawler G, Sturgis J, Rajwa B, Melendez JA *et al.* Mitochondrial complex I inhibitor rotenone induces apoptosis through enhancing mitochondrial reactive oxygen species production. *J Biol Chem* 2003; **278**: 8516–8525.
16. Gao HM, Hong JS, Zhang W, Liu B. Distinct role for microglia in rotenone-induced degeneration of dopaminergic neurons. *J Neurosci* 2002; **22**: 782–790.
17. Pan T, Rawal P, Wu Y, Xie W, Jankovic J, Le W. Rapamycin protects against rotenone-induced apoptosis through autophagy induction. *Neuroscience* 2009; **164**: 541–551.
18. Chen Y, McMillan-Ward E, Kong J, Israels SJ, Gibson SB. Mitochondrial electron-transport-chain inhibitors of complexes I and II induce autophagic cell death mediated by reactive oxygen species. *J Cell Sci* 2007; **120**: 4155–4166.
19. Mader BJ, Pivtoraiko VN, Flippo HM, Klocke BJ, Roth KA, Mangieri LR *et al.* Rotenone inhibits autophagic flux prior to inducing cell death. *ACS Chem Neurosci* 2012; **3**: 1063–1072.
20. Jeong WJ, Rho JH, Yoon YG, Yoo SH, Jeong NY, Ryu WY *et al.* Cytoplasmic and nuclear anti-apoptotic roles of alphaB-crystallin in retinal pigment epithelial cells. *PLoS One* 2012; **7**: e45754.
21. Noh SJ, Jeong WJ, Rho JH, Shin DM, Ahn HB, Park WC *et al.* Sensitization of RPE cells by alphaB-crystallin siRNA to SAHA-induced stage 1 apoptosis through abolishing the association of alphaB-crystallin with HDAC1 in SC35 speckles. *Invest Ophthalmol Vis Sci* 2008; **49**: 4753–4759.
22. Goncalves AP, Maximo V, Lima J, Singh KK, Soares P, Videira A. Involvement of p53 in cell death following cell cycle arrest and mitotic catastrophe induced by rotenone. *Biochim Biophys Acta* 2011; **1813**: 492–499.
23. Dekker PB, Kuipers-Dijkshoorn N, Hogendoorn PC, van der Mey AG, Cornelisse CJ. G2M arrest, blocked apoptosis, and low growth fraction may explain indolent behavior of head and neck paragangliomas. *Hum Pathol* 2003; **34**: 690–698.
24. Maskey D, Yousefi S, Schmid I, Zlobec I, Perren A, Friis R *et al.* ATG5 is induced by DNA-damaging agents and promotes mitotic catastrophe independent of autophagy. *Nat Commun* 2013; **4**: 2130.
25. de Bruin EC, Medema JP. Apoptosis and non-apoptotic deaths in cancer development and treatment response. *Cancer Treat Rev* 2008; **34**: 737–749.
26. Vakifahmetoglu H, Olsson M, Zhivotovsky B. Death through a tragedy: mitotic catastrophe. *Cell Death Differ* 2008; **15**: 1153–1162.
27. Galluzzi L, Vitale I, Abrams JM, Alnemri ES, Baehrecke EH, Blagosklonny MV *et al.* Molecular definitions of cell death subroutines: recommendations of the Nomenclature Committee on Cell Death 2012. *Cell Death Differ* 2012; **19**: 107–120.
28. Vitale I, Galluzzi L, Castedo M, Kroemer G. Mitotic catastrophe: a mechanism for avoiding genomic instability. *Nat Rev Mol Cell Biol* 2011; **12**: 385–392.
29. Erenpreisa J, Kalejs M, Ianzini F, Kosmacek EA, Mackey MA, Emzinsh D *et al.* Segregation of genomes in polyploid tumour cells following mitotic catastrophe. *Cell Biol Int* 2005; **29**: 1005–1011.
30. Puig PE, Guilly MN, Bouchot A, Droin N, Cathelin D, Bouyer F *et al.* Tumor cells can escape DNA-damaging cisplatin through DNA endoreduplication and reversible polyploidy. *Cell Biol Int* 2008; **32**: 1031–1043.
31. Nakada K, Inoue K, Ono T, Isobe K, Ogura A, Goto Y *et al.* Inter-mitochondrial complementation: mitochondria-specific system preventing mice from expression of disease phenotypes by mutant mtDNA. *Nat Med* 2001; **7**: 934–940.
32. Schweers RL, Zhang J, Randall MS, Loyd MR, Li W, Dorsey FC *et al.* NIX is required for programmed mitochondrial clearance during reticulocyte maturation. *Proc Natl Acad Sci* 2007; **104**: 19500–19505.
33. Kundu M, Lindsten T, Yang CY, Wu J, Zhao F, Zhang J *et al.* Ulk1 plays a critical role in the autophagic clearance of mitochondria and ribosomes during reticulocyte maturation. *Blood* 2008; **112**: 1493–1502.
34. Sandoval H, Thiagarajan P, Dasgupta SK, Schumacher A, Prchal JT, Chen M *et al.* Essential role for Nix in autophagic maturation of erythroid cells. *Nature* 2008; **454**: 232–235.
35. Zhang J. Autophagy and mitophagy in cellular damage control. *Redox Biolgy* 2013; **1**: 19–23.
36. Narendra D, Tanaka A, Suen DF, Youle RJ. Parkin is recruited selectively to impaired mitochondria and promotes their autophagy. *J Cell Biol* 2008; **183**: 795–803.
37. Dastgheib K, Green WR. Granulomatous reaction to Bruch's membrane in age-related macular degeneration. *Arch Ophthalmol* 1994; **112**: 813–818.
38. Schultz DW, Weleber RG, Lawrence G, Barral S, Majewski J, Acott TS *et al.* HEMICENTIN-1 (FIBULIN-6) and the 1q31 AMD locus in the context of complex disease: review and perspective. *Ophthalmic Genet* 2005; **26**: 101–105.
39. Mosieniak G, Sikora E. Polyploidy: the link between senescence and cancer. *Curr Pharm Des* 2010; **16**: 734–740.
40. Wang AL, Lukas TJ, Yuan M, Neufeld AH. Increased mitochondrial DNA damage and down-regulation of DNA repair enzymes in aged rodent retinal pigment epithelium and choroid. *Mol Vis* 2008; **14**: 644–651.